A new age-dating model for cool main sequence stars that combines stellar evolution models with gyrochronology

Ruth Angus[1,2,3], Timothy D. Morton[4,2,], Stephen Kane[5], *et al.* (TBD)

ABSTRACT

[1]American Museum of Natural History, Central Park West, Manhattan, NY

[2]Center for Computational Astrophysics, Flatiron Institute, 162 5th Avenue, Manhattan, NY

[3]Department of Astronomy, Columbia University, NY, NY

[4]Department of Astronomy, University of Florida, Gainesville, FL

[5]Department of Physics and Astronomy, UC Riverside, Riverside, CA

Age is the most difficult fundamental stellar property to measure for cool stars on the main sequence, however rotation periods can be used to predict the ages of these stars precisely via gyrochronology. Classical stellar evolution models are not able to predict precise stellar ages on the main sequence, but they can provide precise ages at main sequence turn off. We present a method and *Python* package, called `stardate`, for inferring stellar ages by combining two different dating methods: gyrochronology and isochrone fitting. This method provides ages with uncertainties no more than 20% across the MS and subgiant branch. This combination of two independent age-dating methods can be applied to a much broader range of stellar masses and evolutionary stages and provides ages that are more precise and accurate than either method in isolation. In this investigation, the observables of main sequence stars that are used to trace core hydrogen burning and stellar evolution on the Hertzprung-Russell diagram (T_{eff}, [Fe/H], log(g), parallax, apparent magnitude and photometric colors) are combined with *Kepler* rotation periods, in a Bayesian framework, to jointly infer stellar ages from both stellar evolution models/isochrone placement and gyrochronology. We show that incorporating rotation periods into stellar evolution models significantly improves the precision of inferred ages on the main sequence. However, since ages predicted with gyrochronology are, in general, much more precise than isochronal ages, care must be taken to ensure the gyrochronology relation being used is accurate. In this study we did not aim to recalibrate or improve upon existing gyrochronology models, our goal was to explore the process of combining two independent dating methods. However, only a slight modification to our algorithm would be required to perform a calibration and, since the code is modular, an updated gyrochronology model could easily replace the one used here in future. This publication is accompanied by open source code for inferring stellar ages for cool main sequence stars and subgiants from spectroscopic parameters and/or apparent magnitudes, parallaxes and rotation periods.

1. Introduction

The formation and evolution of the Milky Way (MW) and the planetary systems within it are two topics of significant interest in astronomy today. Both of these fields require precise and accurate ages for tens to hundreds of thousands of stars, however, age is the

most difficult stellar property to measure. The difficulty of age-dating is particularly acute for low mass (GKM) stars on the MS: precisely those that comprise the majority of known planet hosts. Using conventional dating methods, uncertainties on the ages of these stars can be as large as the age of the Universe, in other words they are completely unconstrained. The stars eligible for *truly* precise age-dating, where age uncertainties can be as low as 10%, are those in nearby open clusters, those with observable acoustic oscillations (asteroseismic stars), those just turning off the MS, and the Sun (see Soderblom 2010, for a review of stellar ages). There are only a few tens of cool, MS stars with precise ages that are suitable for exoplanet population studies, however *tens-of-thousands* of precise ages are needed to study the evolution of planetary systems (*e.g.* Petigura et al. 2013; Foreman-Mackey et al. 2014; Veras et al. 2015; Burke et al. 2015). The number of planets detected in open clusters, and therefore with precise ages, is growing (*e.g.* Mann et al. 2017; Rizzuto et al. 2018; Vanderburg et al. 2018; Mann et al. 2018), however there are still only a couple of dozen of these discovered so far and the total number of detectable planets in clusters is unlikely to reach statistical numbers in the near future, if ever. In order to study the evolution of planetary systems, a significant number of precise ages for cool MS *field* stars are needed. Neither cluster stars nor asteroseismic stars can currently provide the numbers required for exoplanet population studies: age-dating methods for cool MS field stars *must* be improved before the evolution of planets can be explored.

The spectra and colors of MS stars do not contain a significant amount of age information because they do not change rapidly. This is represented in the spacing of isochrones on a Hertzsprung-Russell (HR) or color-magnitude diagram (CMD). On the MS, isochrones are tightly spaced and, even with very precise measurements of effective temperature and luminosity, the position of a MS star on the HR diagram may be consistent with range of isochrones spanning several billion years. At main sequence turn-off however, isochrones are spread further apart, so that sufficiently precisely measured temperatures and luminosities may yield ages that are extremely precise. The classical method for measuring stellar ages is called isochrone placement, or isochrone fitting, where surface gravity changes resulting from fusion in the core (usually observed via luminosity, L, and effective temperature, T_{eff}, or absolute magnitude and colour) are compared with a set of models that trace stellar evolution across the HR diagram, or CMD. Surface gravity changes have been thoroughly mapped with physical models, and can be used to calculate relatively accurate (but not necessarily precise) ages, barring some small, $\sim 10\%$ variations between different models (*e.g.* Yi et al. 2001; Dotter et al. 2008; Dotter 2016). Isochronal ages *can* be precise for stars turning off the MS, because the rate of change in brightness and temperature is large during this phase of stellar evolution. However, on the MS itself, there is little differentiation between stars of different ages in the L and T_{eff} plane, so ages tend to be very imprecise. The

method of inferring a star's age from its rotation period, called 'gyrochronology', is much better suited for measuring ages on the MS because MS, stars spin down relatively rapidly.

Magnetic braking in MS stars was first observed by Skumanich (1972) who, studying young clusters and the Sun, found that the rotation periods of Solar-type stars decay with the square-root of time. It has since been established that the rotation period of a star depends, to first order, only on its age and mass (*e.g.* Barnes 2003). This means that by measuring a star's rotation period and a suitable mass proxy (B-V color is commonly used), one can determine its age. The convenient characteristic of stars that allows their ages to be inferred from their *current* rotation periods and independently of their primordial ones, comes from the steep dependence of spin-down rate on rotation period (Kawaler 1989). This means that a star spinning with high angular velocity will experience a much greater angular momentum loss rate than a slowly spinning star. For this reason, no matter the initial rotation period of a Sun-like star, after around the age of the Hyades (500-700 million years) stellar rotation periods appear to converge onto a tight sequence (Irwin and Bouvier 2009). After this time, the age of a star can be inferred, to first order, from its mass and rotation period alone and this is the principle behind gyrochronology.

The relation between age, rotation period and mass has been studied in detail, and several different models have been developed to capture the rotational evolution of Sun-like stars. Some of these models are theoretical and based on physical processes; modeling angular momentum loss as a function of stellar properties as well as the properties of the magnetic field and stellar wind (Kawaler 1988, 1989; van Saders and Pinsonneault 2013; Matt et al. 2015; van Saders et al. 2016). Other models are empirical and capture the behavior of stars from a purely observational standpoint, using simple functional forms that can reproduce the data (Barnes 2003, 2007; Mamajek and Hillenbrand 2008; Angus et al. 2015). Both types of model, theoretical and empirical, must be calibrated using observations. Old calibrators are especially important because new evidence suggests that rotational evolution goes through a transition at old age or, more specifically, at a large Rossby number, Ro (the ratio of rotation period to the convective overturn timescale). For example, old *Kepler* asteroseismic stars rotate more rapidly than expected given their age (*e.g.* Angus et al. 2015; van Saders et al. 2016). A new physically motivated gyrochronology model, capable of reproducing these data, was recently introduced (van Saders et al. 2016). It relaxes magnetic breaking at a critical Rossby number of around the Solar value, 2.1. This model predicts that, after stellar rotation periods lengthen enough to move stars cross this Ro threshold, stars stop spinning down and maintain a constant rotation period from then until they evolve off the MS. The implication is that the ages of stars with $Ro > 2.1$ cannot be measured from their rotation periods.

The gyrochronology models that capture post Ro-threshold, rotational evolution (van Saders et al. 2016) are the current state-of-the-art in rotation dating. These models are expensive to compute and, just as with most isochrones and stellar evolution tracks, are usually pre-computed over a grid of stellar parameters, then interpolation is used to predict the age of a star. The process of measuring a stellar age with these models is similar to inferring an age using any set of isochrones, with the main difference being that rotation period is an additional dimension. Ages calculated using these models are therefore likely to be much more precise than using rotation-free isochrones since rotation period provides an additional anchor-point for the age of a star. We present here a complementary method that combines isochrones with an *empirical* gyrochronology model using a Bayesian framework. The methodology is related to the models described above (van Saders et al. 2016) in that both use a combination of rotation periods and other observable properties that track stellar evolution on the HR diagram in concert. The main difference is that the gyrochronology model used here is an entirely empirically calibrated one, as opposed to a physically derived one. One major advantage of using a physically motivated gyrochronology model over an empirically calibrated one is the ability to rely on physics to interpolate or extrapolate over parts of parameter space with sparse data coverage. However, rotational spin-down is a complex process that is not yet fully understood and currently no physical model can accurately reproduce all the data available. For this reason, even physically motivated gyrochronology models cannot always be used to reliably extrapolate into unexplored parameter space. Physical models, when calibrated to data can provide insight into the physics of stars however, if accurate and precise *prediction* of stellar properties is desired, empirical models can have advantages over physical ones. For example, the data may reveal complex trends that cannot be reproduced with our current understanding of the physical processes involved but may be captured by more flexible data-driven models. In addition, it is relatively straightforward to build an element of stochasticity into empirical models, *i.e.* to allow for and incorporate outliers or noisy trends. This may be particularly important for stellar spin down, which does not always seem to behave predictably. A further advantage of empirical models is that inference is more tractable: it can be extremely fast to fit them to data. We use a simple, empirical, deterministic gyrochronology model in this work, which, like any other gyrochronology model, cannot yet reproduce all the observed data. Simple modifications could be made to this model to produce significant improvements, for example, by including instrinsic scatter and outliers, however we leave these improvements for a future project. Ultimately, the model we present here will provide a baseline against which other gyrochronology models can be compared.

This paper is laid out as follows. In section 2 we provide additional motivation for combining gyrochronology and isochrone fitting by providing examples based on information

theory. In section 3 we describe our new age-dating model and its implementation, in section 4 we test this model on simulated stars, cluster stars and asteroseismic stars, and in section 5 we discuss the implications of these tests and future pathways for development. Throughout this paper we use the term *'observables'* to refer to the following observed properties of a star, T_{eff}, $\log(\mathrm{g})$, observed bulk metallicity ($[\hat{F}]$), parallax ($\bar{\omega}$), photometric colors in different passbands ($\mathbf{m_x} = [m_J, m_H, m_K, m_B, m_V, m_G, ...]$, etc) and rotation period (P_{rot}). The term *'parameters'* refers to the physical properties of that star: age (A), mass (M), true bulk metallicity (F), distance (D) and V-band extinction (A_V). These are the properties that generate the observables.

2. Combining isochrone fitting with Gyrochronology: Motivation

In order to demonstrate why a combination of gyrochronology and isochrone fitting can provide more precise ages than either method used in isolation, we calculated the information provided by each method for a range of stellar masses, ages and evolutionary stages.

According to observations of cluster stars and the Sun, the decrease in rotation period with time is roughly proportional to the inverse square root of age, $\frac{dP_{\rm rot}}{dt} \propto {\rm Age}^{-n}$, where n∼0.5. This corresponds to a large rate of change relative to typical rotation period measurement uncertainties. For example, the Sun's rotation period is currently decreasing at a rate of around 3 days per billion years (unless it has already stopped spinning down, *e.g.* van Saders et al. 2016), and the 1 billion year-old Sun spun down at a rate of around 6 days per billion years. These are relatively large changes compared with the average uncertainties on rotation period measurements: the median rotation period uncertainty in the McQuillan et al. (2014) catalog is around 0.1 days. In contrast, the temperature of a K dwarf changes by about 20 K every billion years which is small compared to typical observational uncertainties of 20-100 K. Rotational isochrones, or 'gyrochrones' provide much more *information* about age than traditional isochrones. The difference in information conveyed by rotation vs $T_{\rm eff}$ and L can be quantified by calculating the time derivatives of a star's observables. The rate of change of $T_{\rm eff}$ and L dictates the minimum theoretically achievable uncertainty on an age inferred via isochrone fitting, given some observational uncertainties. Similarly, the rate of change of rotation period dictates the minimum achievable uncertainty on an age inferred via gyrochronology. In order to quantify the minimum theoretical uncertainty on ages calculated via isochrone fitting and gyrochronology, we calculated the Fisher information for the MIST isochrones (Paxton et al. 2011, 2013, 2015; Dotter 2016; Choi et al. 2016; Paxton et al. 2018) and an empirical polynomial gyrochronology model we fit to the Praesepe cluster. The Fisher information quantifies the amount of information that an observable imparts onto an unknown parameter. In the case of isochrone fitting on a CMD using *Gaia* data, the observables are *Gaia* absolute magnitude M_G and color, $G_{BP} - G_{RP}$ and the parameter is age, or time, t. The Fisher information is the variance of the parameter, t, given the covariance of the observables and their derivatives with respect to t. The inverse covariance matrix of the parameters (in this case we have just one parameter, age or time, t), given the covariance matrix of the data, $\mathbf{y} = [M_G, G_{BP} - G_{RP}]$, is given by the following equation,

$$C_{\rm Age}^{-1} = \left[\frac{d\mathbf{y}}{dt}\right]^T C_{\mathbf{y}}^{-1} \left[\frac{d\mathbf{y}}{dt}\right]. \tag{1}$$

Since we just have one parameter, $C_{\rm Age}^{-1}$ is a scalar, the inverse variance of age, $\sigma_{\rm Age}^{-2}$. In order to calculate the age uncertainty from the MIST isochrones, we calculated numerical derivatives of $\frac{dG}{dt}$, and $\frac{d(G_{BP}-G_{RP})}{dt}$ at every point on the MIST model grids. We then calculated the

isochronal age uncertainty, σ_{Age} at every point on the grid. Figure 1 shows Solar-metallicity MIST isochrones, colored by σ_{Age}.

Figure 1 shows the minimum theoretical absolute age uncertainty, σ_{Age} (left panel), calculated using typical uncertainties on *Gaia* absolute magnitude, M_G, and color, $G_{BP}-G_{RP}$ represented as black errorbars in the top right corner. The typical *Gaia* uncertainties are 0.5 in both M_G and $G_{BP}-G_{RP}$. These estimates are based on a calculation of the median uncertainty on *Gaia* absolute G-magnitude of cool stars which is dominated by the parallax uncertainty. We assumed the same uncertainty on $G_{BP}-G_{RP}$. The minimum uncertainty on isochronal age ranges from around 10 million years at MS turn off (upper left yellow area) to around the age of the Universe for K dwarfs (middle to lower-right blue area). The minimum *relative* age uncertainty, $\sigma_{\text{Age}}/\text{Age} \times 100$, plotted in the right-hand panel ranges from less than 1% for old MS turn off stars with ages around 13 Gyr and age uncertainties less than 0.1 Gyr, up to tens-of-thousands of percent for the youngest K and M dwarfs with unconstrained ages.

We also calculated the Fisher information for a *combined isochronal and gyrochronology model*. In this case we effectively had four observables: M_G and $G_{BP}-G_{RP}$, determined by the MIST isochrones; and P_{rot} (rotation period) and $G_{BP}-G_{RP}$ *again*, this time determined by the gyrochronology model. We used a simple gyrochronology model, calibrated by fitting a fourth-order polynomial in rotation period-*Gaia* color space and a first order polynomical in rotation period-age space to the 650 Myr Praesepe cluster and the Sun, only. This model is described in more detail later in this section. We calculated analytic derivatives for $\frac{dP_{\text{rot}}}{dt}$ and $\left(\frac{d(G_{BP}-G_{RP})}{dt}\right)_{\text{gyro}}$ and combined these with the numerical derivatives of $\frac{dG}{dt}$ and $\left(\frac{d(G_{BP}-G_{RP})}{dt}\right)_{\text{iso}}$ in order to calculate the total age uncertainty, $\sigma_{\text{Age (iso \& gyro)}}$. Figure 2 shows Solar-metallicity MIST isochrones, colored by $\sigma_{\text{Age (iso \& gyro)}}$. The results are presented the same way as figure 1 however, figure 2 shows age uncertainties calculated using isochrones *and a polynomial gyrochronology model*. The age uncertainties were calculated using typical *Gaia* M_G and $G_{BP}-G_{RP}$ uncertainties, represented as black errorbars in the top right corner, and rotation period uncertainties of 1 day. The minimum theoretical absolute age uncertainty inferred using gyrochronology and isochrone fitting simultaneously, $\sigma_{\text{Age (iso \& gyro)}}$ (left panel of figure 2), ranges from tens of millions of years for stars at MS turn off to a few billion years (up to around 3 Gyr for old G dwarfs). The very precise ages at MS turn off are still provided by isochrone fitting – the incredible precision achievable with isochrone fitting at MS turn off dominates over the precision provided by gyrochronology. On the MS however, gyrochronology provides extremely precise ages and its precision dominates over isochrone fitting. The gyrochronology model used to calculate the Fisher information is not appropriate for stars turning off the MS as it does not account for a

rapid decrease in rotation period that may be caused by the stellar radius increasing (see van Saders and Pinsonneault 2013). The right-hand panel of figure 2 shows the *relative* age uncertainty achievable with joint isochronal and gyrochronal age inference. Relative age uncertainty, $\text{Age}/\sigma_{\text{Age (iso \& gyro)}} \times 100$ ranges from less than 1% at MS turn off, where isochrones provide precise ages because they are widely spaced, to a maximum of around 30% for young G dwarfs, where gyrochrones are at their most tightly spaced. The dramatic improvement in age precision seen across the MS when gyrochronology is used provides the motivation for combining isochrone fitting with gyrochronology. The minimum relative age uncertainty for GKM stars on the MS is typically around 20% – gyrochronology predicts precise ages for these kinds of stars. 20% age precision for gyrochronology was also predicted in previous studies. (**?**). Gyrochronology and isochrone fitting are extremely complementary: gyrochronology contributes most of the precision on the MS because rotation period information dominates over color and luminosity information, however it is not applicable to hot stars without deep convection zones and evolved stars. These are precisely the stars optimally fitted with isochrone models.

An important caveat of this demonstration is that this is the minimum theoretical precision given the *adopted* gyrochronology model and, since the model used for this calculation does not include intrinsic scatter (which is particularly large for young stars), these minimum age uncertainty calculations are over-optimistic, especially for young stars. Similarly, our model does not account for weakened magnetic braking at old ages (van Saders et al. 2016) so is also optimistic for old dwarfs. Still, figures 1 and 2 provide an idea of the improvement provided by gyrochronology over isochrone fitting alone.

In order to calculate analytic derivatives of the gyrochronology model, we fit a linear model to the Praesepe open cluster and the Sun (see figure 6. We used a three-dimensional polynomial model to predict age as a function of *Gaia* color and rotation period for Praesepe and the Sun. This model consists of a 4th order polynomial in logarithmic Gaia color: $G_{BP} - G_{RP}$, which we write as C_G for simplicity, and a 1st order polynomial (a straight line) in logarithmic age. For this analysis, rotation periods for Praesepe were obtained from Douglas et al. (2017) and their *Gaia* colors were obtained by crossmatching their sky-projected positions with the *Gaia* DR2 catalog. When fitting this gyrochronology model, we chose to make *age* the dependent variable because the uncertainties on stellar age are much greater than the uncertainties on rotation period. We fit the following model to Praesepe members:

$$\log_{10}(A) = a + b \log_{10}(C_G) + c \log_{10}^2(C_G) + d \log_{10}^3(C_G) + e \log_{10}^4(C_G) + f \log_{10}(P) \quad (2)$$

where P is rotation period in days, C_G is Gaia color, A is stellar age in years and the lower case letters are free parameters. We adopted an age for Praesepe of 650 ± 100 million years

(Fossati et al. 2008; Gossage et al. 2018), a Solar age of 4.56 ± 0.01 Gyr (Connelly et al. 2012), and a Solar rotation period of 26 days (Balthasar et al. 1986; Howe et al. 2000, Morris *et al.*, in prep). The Sun's color in the Gaia color is 0.82 (Casagrande and VandenBerg 2018). We found best-fit values: $a = 7.37 \pm 0.03$, $b = -1.4 \pm 0.1$, $c = 5.0 \pm 0.8$, $d = -34 \pm 3$, $e = 66 \pm 14$, and $f = 1.49 \pm 0.02$. This model and the data it was fit to are plotted in figure 6. To be clear, this model was only used to calculate the Fisher information and produce figures 1 and 2, because it has simple analytic derivatives. Since it was only fit to a single cluster and the Sun it is not generally applicable and was not used in any other aspects of the analysis performed in this paper. The gyrochronology model used throughout the rest of the analysis is described in section 3 and equation 13.

Fig. 1.— This figure shows Solar-metallicity MIST isochrones in *Gaia* absolute G-band magnitude and Gaia $G_{BP} - G_{RP}$ color. In the left panel the isochrones are colored by the minimum absolute age uncertainty at each point on the CMD, calculated using the Fisher information, based on the typical uncertainties of *Gaia* photometry (represented by black errorbars in the upper right). The Sun's position (Casagrande and VandenBerg 2018) is indicated with the Solar symbol. The purple color in the top left corresponds to small age uncertainties, *i.e.* good age precision. Age precision increases as stars begin to turn off the MS. On the MS however, particularly at low masses, the age precision is poor. For late K dwarfs, for example, isochrone fitting age uncertainties exceed the age of the Universe. This makes sense when you consider that typical *Gaia* uncertaintes on G and $G_{BP} - G_{RP}$ exceed the entire width of the MS, which spans 0.01-14 Gyrs. Isochrone fitting is not an appropriate age-dating method for MS stars, especially at low masses. In the right panel the isochrones are colored by the logarithmic *relative* age precision at each point in the CMD. Relative age uncertainties range from 100% for the oldest MS GKM stars, to several thousand percent for the youngest. These age uncertainties were calculated using the derivatives of G and $G_{BP} - G_{RP}$ with age, *i.e.* the rate of change in a star's luminosity and temperature. For example, K dwarf temperatures increase at a rate of only around 20 K per billion years. The precision with which an age can be measured is related to the separation between isochrones, which indicate epochs of rapid change (steep gradients).
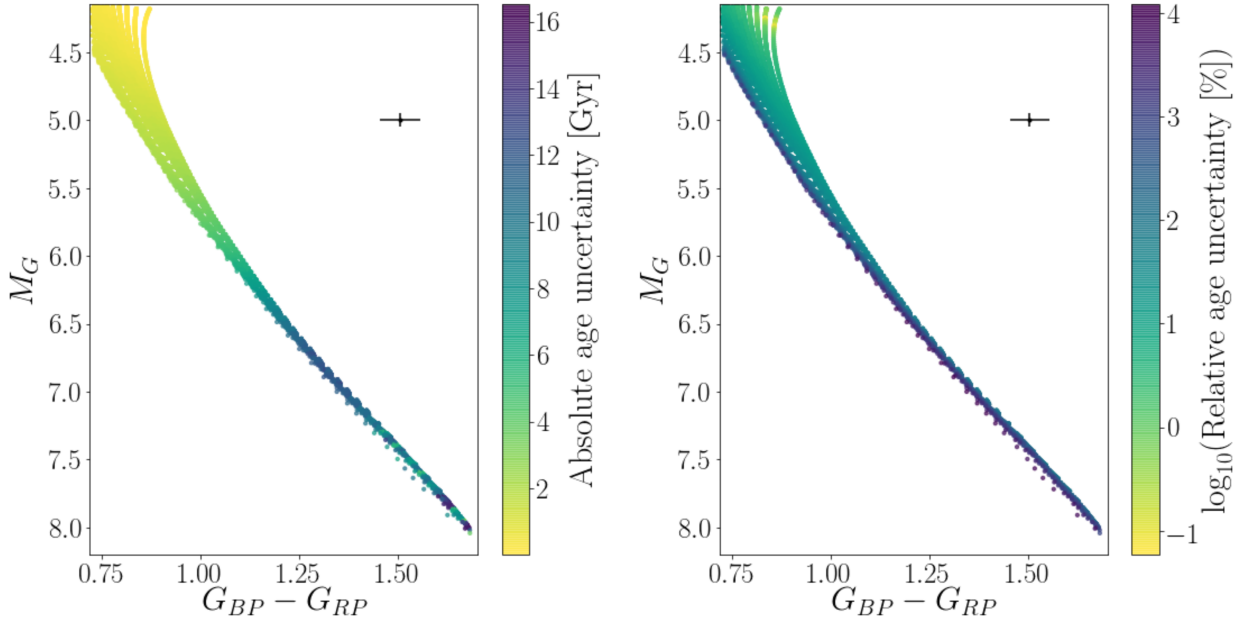
Fig. 2.— As figure 1, however in this case the minimum age uncertainties are calculated based on isochrone fitting and gyrochronology *combined*. The isochrones are colored by the minimum relative age uncertainty at each point on the CMD, based on the typical uncertainties of Gaia photometry and Kepler rotation period uncertainties (assumed to be around 1 day). In contrast to figure 1, here the left panel shows the *logarithmic* absolute age and the right panel shows the linear relative age. The isochrones still supply precise ages at the MS turn off (purple, upper left) however, gyrochronology supplies precise ages on the MS (15 - 25% relative precision). Gyrochronology and isochrone fitting complement each other and when used together, all subgiants and MS stars can have ages more precise than 30%.
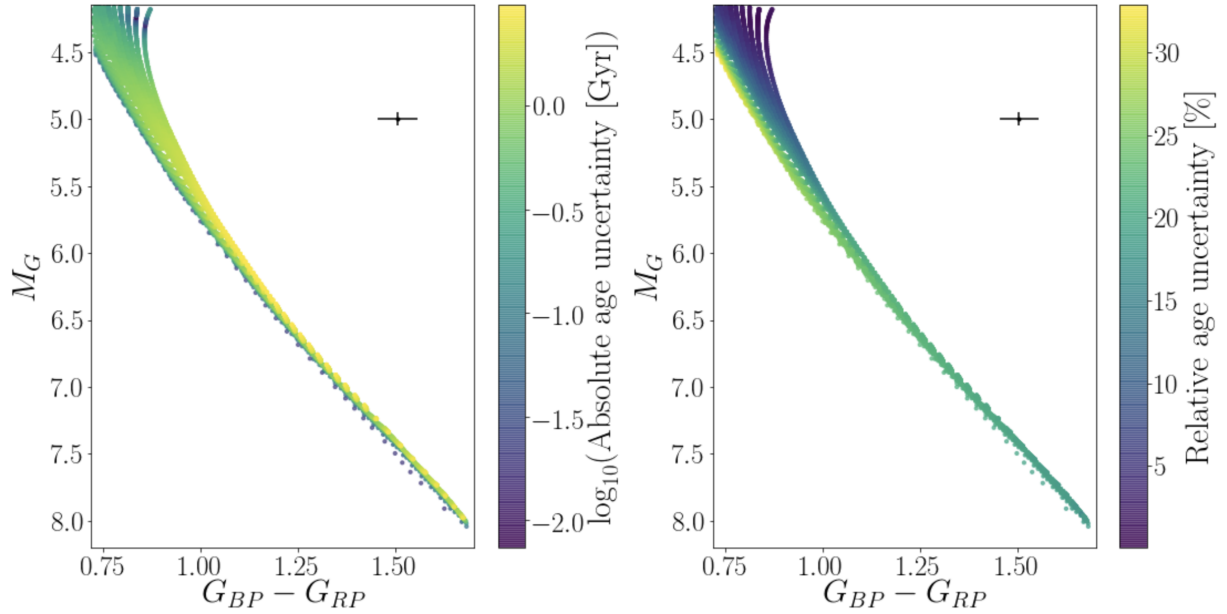
3. Method

In this section we describe our combined isochrone fitting and gyrochronology model. A common approach to stellar age-dating is to make separate age predictions using separate sets of observables. For example, if a star's rotation period, parallax, and apparent magnitudes in a range of bandpasses are available, it is possible to predict its age from both gyrochronology and isochrone fitting separately. How these two age predictions are later combined is then a difficult choice. Is it best to average these predictions, to use the more precise of the two, or the one believed to be more accurate? The methodology described here provides an objective method for combining age estimates. There is, after all, only one age for each star. In Bayesian statistics, combining information from different models can be relatively simple, as long as the processes being modeled; those that generated the data, are independent. In this case, we are combining information that relates to the burning of hydrogen in the core (this is the process that drives the slow increase in T_{eff} and luminosity over time) with information about the magnetic braking history of a star (the current rotation period). We can assume that, to first order, these two processes are independent: the hydrogen fraction in the core does not affect a star's rotation period and vice versa. In practise, we can never be entirely sure that two such processes are independent but, at least within the uncertainties, any dependence here is unlikely to affect our results. If this assumption is valid, the likelihoods calculated using each model can be multiplied together.

The desired end product of this method is an estimate of the non-normalized posterior probability density function (PDF) over the age of a star,

$$p(A|\mathbf{m_x}, T_{\text{eff}}, \log(g), \hat{F}, P_{\text{rot}}, \bar{\omega}), \tag{3}$$

where A is age, $\mathbf{m_x}$ is a vector of apparent magnitudes in various bandpasses, $\hat{F}$ is the *observed* bulk metallicity, P_{rot} is the rotation period and $\bar{\omega}$ is parallax. In order to calculate a posterior PDF over age, we must marginalize over parameters that relate to age, but are not of interest in this study: mass (M), distance (D), V-band extinction (A_V) and the *inferred* bulk metallicity, F. The marginalization involves integrating over these extra parameters,

$$p(A|\mathbf{m_x}, T_{\text{eff}}, \log(g), \hat{F}, P_{\text{rot}}, \bar{\omega}) \tag{4}$$
$$\propto \int p(\mathbf{m_x}, T_{\text{eff}}, \log(g), \hat{F}, P_{\text{rot}}, \bar{\omega}|A, M, D, A_V, F) \ p(A)p(M)p(D)p(A_V)p(F)dMdDdA_VdF.$$

This equation is a form of Bayes' rule,

$$\text{Posterior} \propto \text{Likelihood} \times \text{Prior}, \tag{5}$$

where the likelihood of the data given the model is,

$$p(\mathbf{m_x}, T_{\text{eff}}, \log(g), \hat{F}, \bar{\omega}, P_{\text{rot}}|A, M, D, A_V, F), \tag{6}$$

and the prior PDF over parameters is,

$$p(A)p(M)p(D)p(A_V)p(F). \tag{7}$$

Not all of the observables on the left of the '|' in the likelihood depend on all of the parameters to the right of it. For example, rotation period, $P_{\rm rot}$ does not depend on V-band extinction, A_V. In our model, we make use of conditional independencies like this and use them to factorize the likelihood. Instead of the likelihood of equation 11, where every observable depends on every parameter, our model can be factorized as,

$$p(\mathbf{m_x}, T_{\rm eff}, \log(g), \hat{F}, \bar{\omega}, C_{B-V}|A, M, D, A_V, F) \; p(P_{\rm rot}|A, C_{B-V}), \tag{8}$$

where we have introduced a new parameter, C_{B-V}, which is the $B - V$ color that is often used as a mass proxy in the literature. In our model C_{B-V} is not measured but *inferred*: it is a latent parameter. We infer C_{B-V} because many stars do not have a directly measured $B - V$ color. For example, most *Kepler* stars have 2MASS photometry in J, H and K bands and *Gaia* photometry in G, G_{BP} and G_{RP}, but do not all have B and V band colors. However, the gyrochronology model we use is calibrated to B-V color, not J-K or otherwise (Barnes 2007; Mamajek and Hillenbrand 2008; Angus et al. 2015). A probabilistic graphical model (PGM) depicting the joint probability over parameters and observables is shown in figure 3. It describes the conditional dependencies between parameters (in white circles) and observables (in grey circles) with arrows leading from the causal processes to the dependent processes. For example, it is the mass, age, metallicity, extinction and distance that determines the observed spectroscopic properties ($T_{\rm eff}$, $\log(g)$, [Fe/H]) and apparant magnitudes, $\mathbf{m_x}$). These parameters also determine the C_{B-V} color of a star. In turn, it is a star's age and C_{B-V} color that determine its rotation period. Note that, written this way, stellar rotation periods do not directly depend on stellar mass. Mass determines C_{B-V} and C_{B-V}, along with age determines rotation period. The purpose of this PGM is not to depict the physical realities of stellar evolution, it is only a visual description of the structure of the model we use here. Breaking up the problem this way allows us to efficiently join isochronology and gyrochronology and infer the joint age of a star from all its observables. It may well be that rotation period depends directly on mass and metallicity in reality, but it is more practical for us to assume that these dependencies are weak enough not to significantly affect the ages that we ultimately infer.

The factorization of the likelihood described in equation 8 and depicted in figure 3 allows us to multiply two separate likelihood functions together: one computed using an isochronal model and one computed using a gyrochronal model. We assume that the probability of observing the measured observables, given the model parameters is a Gaussian and that the

observables are identically and independently distributed. These assumptions allow us to use Gaussian likelihood functions. The isochronal likelihood function is,

$$\mathcal{L}_{\text{iso}} = p(\mathbf{m_x}, T_{\text{eff}}, \log(g), \hat{F}, \bar{\omega}, C_{B-V} | A, M, D, A_V, F) \qquad (9)$$
$$= \frac{1}{\sqrt{(2\pi)^n \det(\Sigma)}} \exp\left(-\tfrac{1}{2}(\mathbf{O_I} - \mathbf{I})^T \Sigma^{-1} (\mathbf{O_I} - \mathbf{I})\right),$$

where $\mathbf{O_I}$ is the n-dimensional vector of n observables: T_{eff}, $\log(g)$, $\hat{F}$, $\bar{\omega}$, $\mathbf{m_x}$ (where n is 4+ the number of apparant magnitudes in different pass-bands that are available) and Σ is the covariance matrix of that set of observables. $\mathbf{I}$ is the vector of *model* observables that correspond to a set of parameters: A, M, F, D and A_V, calculated using an isochrone model. We assume there is no covariance between these observables and so this covariance matrix consists of individual parameter variances along the diagonal with zeros everywhere else. The gyrochronal likelihood function is,

$$\mathcal{L}_{\text{gyro}} = p(P_{\text{rot}} | A, C_{B-V}) \qquad (10)$$
$$= \frac{1}{\sqrt{(2\pi) \det(\Sigma_P)}} \exp\left(-\tfrac{1}{2}(\mathbf{P_O} - \mathbf{P_P})^T \Sigma^{-1} (\mathbf{P_O} - \mathbf{P_P})\right),$$

where $\mathbf{P_O}$ is a 1-D vector of observed rotation periods, $\mathbf{P_P}$ is the vector of corresponding predicted rotation periods, calculated using the vector of ages and C_{B-V} values that correspond to the input parameters as predicted by the isochronal model. The full likelihood function used in our model is the product of these two likelihood functions,

$$\mathcal{L}_{\text{full}} = \frac{1}{\sqrt{(2\pi)^n \det(\Sigma)}} \exp\left(-\tfrac{1}{2}[\mathbf{O_I} - \mathbf{I}]^T \Sigma^{-1} [\mathbf{O_I} - \mathbf{I}]\right) \qquad (11)$$
$$\times \frac{1}{\sqrt{(2\pi) \det(\Sigma_P)}} \exp\left(-\tfrac{1}{2}[\mathbf{P_O} - \mathbf{P_P}]^T \Sigma^{-1} [\mathbf{P_O} - \mathbf{P_P}]\right).$$

We place priors over the model parameters A, M, F, D and A_V. These priors represent our 'prior beliefs' about the values these parameters will take, before we use the data to update those beliefs via a likelihood and produce a 'posterior' belief about their values. These priors are described in the appendix.

To calculate $\mathbf{I}$, the vector of predicted isochronal observables, we use the `isochrones.py` *python* package which has a range of functionalities relating to isochrone fitting. The first of the `isochrones.py` functions we use is the likelihood function of equation **??**. The `isochrones.py` likelihood function accepts a dictionary of observables which can, but does not *have* to include, all of the following: T_{eff}, $\log(g)$, F, parallax and apparent magnitudes in a range of colors, as well as the uncertainties on all these observables. It then calculates the residual vector $(\mathbf{O_I} - \mathbf{I})$ where $\mathbf{O_I}$ is the vector of observables and $\mathbf{I}$ is a vector of corresponding predicted observables. The prediction is calculated using a set of isochrones

(we use the MIST models, Paxton et al. 2011, 2013, 2015; Dotter 2016; Choi et al. 2016; Paxton et al. 2018), where the set of *model* observables that correspond to a set of physical parameters is returned. This requires interpolation over the model grids since, especially at high dimensions, it is unlikely that any set of physical parameters will exactly match a precomputed set of isochrones. The observables that correspond to a set of physical parameters go into $\mathbf{I}$ and the `isochrones.py` likelihood function returns the result of equation **??**. The second `isochrones.py` function we use is one that predicts C_{B-V} for a given set of stellar parameters. This color is then used to calculate the gyrochronal likelihood function of equation 10.

The inference processes procedes as follows (as a reminder, we use *observables* to refer to the data: T_{eff}, log(g), etc and *parameters* to refer to the model parameters: age, mass, etc). First, a set of parameters: age, mass, true bulk metallicity, distance and extinction, as well as observables T_{eff}, log(g), bulk metallicity, 2MASS colors and parallax ($\mathbf{O_I}$) for a single star are passed to the isochronal likelihood function (equation **??**). Then, a set of *model* values of T_{eff}, log(g), bulk metallicity, apparent magnitudes and parallax ($\mathbf{I}$) that correspond to that set of parameters are calculated by `isochrones.py`. The isochronal log-likelihood, $\ln(\mathcal{L}_{\text{iso}})$, is then computed for these parameter values. The same age that was passed to the likelihood function, and the C_{B-V} corresponding to it, along with the observed rotation period, are then passed to the gyrochronal likelihood function (equation 10). The gyrochronal log-likelihood, $\ln(\mathcal{L}_{\text{gyro}})$, is computed. The full log-likelihood is then calculated,

$$\ln(\mathcal{L}_{\text{full}}) = \ln(\mathcal{L}_{\text{iso}}) + \ln(\mathcal{L}_{\text{gyro}}), \tag{12}$$

and added to the log-prior to produce a single sample from the posterior PDF.

When applying our model to infer the age of a star, we sampled the joint posterior PDF over age, mass, metallicity, distance and extinction using the affine invariant ensemble sampler, `emcee` (Foreman-Mackey et al. 2013) with 24 walkers. Samples were drawn from the posterior PDF until 100 *independent* samples are obtained. We actively estimated the autocorrelation length, which indicates how many steps are taken per independent sample, after every 100 steps using the autocorrelation tool built into `emcee`. The MCMC concluded when *either* 100 times the autocorrelation length was reached and the change in autocorrelation length over 100 samples was less than 0.01, *or* the maximum of 100,000 samples was obtained. This method is trivially parallelizable, since the inference process for each star can be performed on a separate core. The age of a single star can be inferred in around one hour on a laptop computer.

The gyrochronology model we used to predict P_P is,

$$P_{\text{rot}} = A^\eta \alpha (C_{B-V} - \delta)^\beta, \tag{13}$$

where $P_{\rm rot}$ is rotation period in days, C_{B-V} is a star's $B - V$ color, A is stellar age in Myrs and η, α, β and δ take values 0.55, 0.4, 0.31 and 0.45 respectively (Angus et al. 2015). This functional form was introduced by (Barnes 2007) and the parameter values are adopted from the recalibration performed in Angus et al. (2015), which is based on young cluster stars and old asteroseismic stars.

It was recently shown that a simple power law in age does not provide a good fit to old asteroseismic stars (Angus et al. 2015; van Saders et al. 2016). It is hypothesized that the magnetic braking of these old stars has ceased and cannot be modeled with a Skumanich-like spin-down law (van Saders et al. 2016). In future, the above model could and should be updated to include a more flexible treatment of rotation period as a function of age in order to account for the change of slope in the relation. Until then, this method should only be used for stars with Rossby number below 2.1 (van Saders et al. 2016), *i.e.* their ratio of rotation period to convection overturn time ($P/\tau = Ro$) does not exceed 2.1. In this work we are chiefly concerned with introducing a new framework where rotation periods are modeled *simultaneously* with isochronal features. Although the gyrochronology models used here do not provide a good fit to all the available data, we reiterate that no single model *is* able to reproduce all the data, and that there is utility in using such a simple, linear, empirical model like this. Again, we are not attempting to improve gyrochronology models in this work: in this paper we are more concerned with introducing a new approach to modeling stellar ages, however, our method is highly flexible and modular and an improved gyrochronology model could easily be swapped in for this one in future. Our model allows a linear combination of other, *physical* parameters to be used to predict age from rotation period, like $\log g$, metallicity and mass. In future, it may be better to model stars in physical rather than observable parameter space.

Fig. 3.— A probabilistic graphical model (PGM) showing the conditional dependencies between the parameters (white nodes) and observables (gray nodes) in our model. θ is a vector of *parameters*: mass, observed bulk metallicity, distance and V-band extinction; and $\mathbf{O}$ is a vector of *observables*: apparent magnitudes, effective temperature, surface gravity, observed bulk metallicity, and parallax. The observables, $\mathbf{O}$, are determined by the parameters, A and θ. C_{B-V} is a latent parameter that is also determined by the parameters A and θ. In our model, the rotation period observable, P, is determined *only* by the age, A, and color C_{B-V} parameters. The dependencies of observables on parameters and parameters on parameters are indicated by arrows that start at a 'parent' node and end at the dependent observable, or 'child' node. In our model, rotation period does not directly depend on distance, extinction, metallicity or mass, only age and B-V color. This PGM is a representation of the factorized joint PDF over parameters and observables of equation 8.
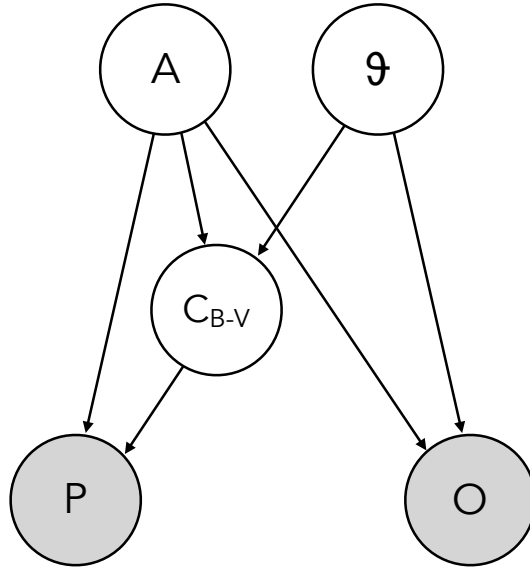
4. Results

In order to demonstrate the performance of our method, we conducted two sets of tests. In the first we simulated a set of observables from a set fundamental parameters for a few hundred stars using the MIST stellar evolution models and a gyrochronology model, then compared the parameters predicted with our model to the true parameters used to generate the data. In the second we tested our model by attempting the measure the ages of individual stars in the Praesepe open cluster and compared the results to the establised age of Praesepe. The age of Praesepe, like any open cluster, has been measured precisely because it is an ensemble of coeval stars with the same metallicity: a single stellar poplulation, and its age can be precisely established through isochrone fitting and MS turn-off. We adopted an age of 650 Myrs for Praesepe (Fossati et al. 2008; Perryman et al. 1998).

4.1. Test 1: simulated stars

For the first test we drew masses, ages, bulk metallicities, distances and extinctions at random for 1000 stars from the following uniform distributions:

$$M \sim U(0.5, 1.5) \ [M_\odot] \tag{14}$$

$$A \sim U(0.5, 14) \ [\text{Gyr}] \tag{15}$$

$$F \sim U(-0.2, 0.2) \tag{16}$$

$$D \sim U(10, 1000) \ [\text{pc}] \tag{17}$$

$$A_V \sim U(0, 1). \tag{18}$$

T_{eff}, log(g), $\hat{F}$, $\bar{\omega}$ C_{B-V} and apparent magnitudes J, H and K were generated, without noise, from these stellar parameters using the MIST stellar evolution models. Rotation periods were generated using the gyrochronology relation of equation 13. We took two approaches to inferring the ages of these simulated stars: firstly using isochrone fitting *only*, and secondly using isochrone fitting *combined with* a gyrochronology model. For all stars, our initial guesses for the parameters were $M = 1M_\odot$, $A = 1$ Gyr, $F = 0$, $D = 500$ pc and $A_V = 0.1$.

Figure 4 shows the results of using isochrone fitting to estimate the posterior PDFs over the stellar ages of simulated stars. True stellar ages are plotted on the x-axis and the posterior PDFs of the inferred ages are plotted on the y-axis. The rotation periods of stars were not incorporated into this model: these posterior PDFs were obtained by isochrone fitting only, using the likelihood function in equation (9). In most cases ages are only weakly constrained by the stellar evolution models and in some cases there is no age constraint: the age of the

star is consistent with all ages from 0-14 Gyrs. This is because stellar temperatures and luminosities do not change rapidly on the main sequence: isochrones are tightly spaced there and, as a result, even precisely measured temperatures and luminosities often do not yield precise ages. Figure 5 shows the results of using isochrones *combined* with a gyrochronology model. These ages were inferred using the likelihood of equations (11)/(12). Again, figure 5 shows true stellar ages on the x-axis and the posterior PDFs of the inferred ages on the y-axis. Here, unlike the isochrone only case, the recovered ages are precise because there is more age information in stellar rotation periods than in effective temperatures and absolute magnitudes. Gyrochronology isochrones (or gyrochrones) are more widely separated relative to the observational uncertainties than the MIST isochrones. Put another way, the rotation periods of two stars of different ages and the same mass will have rotation periods that differ significantly – almost certainly more than the observational uncertainty on rotation period. On the other hand, such stars are likely to have extremely similar luminosities and temperatures and the differences between these properties are likely to be smaller than the observational uncertainties.

Figures **??** and **??** show the simulated stars on a color magnitude diagram, colored by the relative precision of their predicted ages. Figure **??** shows age precision as a function of CMD position using isochrone fitting only, and figure **??** shows age precision using isochrone fitting and gyrochronology combined. These figures are semi-empirical versions of figures **??** and **??**, which were created using information theory, and show the theoretical minimum precision of isochrone fitting and gyrochronology. Still to do: add these figures!

This simulation experiment is unrealistic for two main reasons: firstly, we simulated data from the same gyrochronology model we used to infer ages and so the results will be perfectly accurate by design. Secondly, we simulated data without any intrinsic scatter built into the gyrochronology model; it is a deterministic model. This means that a rotation period and color predicts a corresponding single-valued age, rather than a probability distribution over ages. This is unrealistic given observations of open clusters whose members clearly show excess scatter in their rotation periods, particularly for less massive stars (see figure 6). These results look precise and accurate, but this is misleading. Inaccuracies would arise if the gyrochronology model was incorrect or poorly calibrated in some areas of parameter space and imprecision would arise if intrinsic scatter were built into the gyrochronology model and/or the observations. The result of using a deterministic model, such as the one used in this experiment, is that the uncertainties on stellar ages will be unrealistically small. We leave the recalibration of gyrochronology models for a future exercise since, in this work, we are mostly interested in testing the results of simply combining gyrochronology and isochrone fitting. The above experiment shows that building gyrochronology into stellar evolution models results in much more precise age predictions, as predicted by information

theory. We have not yet made any statement about accuracy however; the above experiment produces accurate ages by construction. In order to test the accuracy of this method, we tested it on real data: the Praesepe open cluster.

4.2. Test 2: the Praesepe Cluster

In order to test our model on real stars with known ages, we selected a sample of cluster stars with precisely measured ages from ensemble isochrone fitting and main sequence turn off. The ages of open clusters can be measured much more precisely than field stars. Stars in the same cluster formed (we assume) from the same molecular cloud at the same time and therefore have the same metallicity and age (to within a few million years). Stars with the same metallicity and age fall on the same isochrone, allowing perfect isochrone selection and providing a $N^{-1/2}$ decrease in uncertainty where N is the number of cluster stars. Single stellar populations also allow main sequence turn off to be identified and, as demonstrated in figure 1, the turn off supplies a large amount of age information. We compiled rotation periods, *Gaia* photometry and *Gaia* parallaxes for members of Praesepe, a ~650 Myr cluster (Fossati et al. 2008). We chose Praesepe because it is relatively tightly clustered on the sky and many of its members were targeted in a single *K2* campaign, from which it was possible to measure rotation periods via frequency analysis of member's light curves (Douglas et al. 2017). We crossmatched Praesepe members with measured rotation periods (Douglas et al. 2017) with the Gaia DR2 catalog (Gaia Collaboration et al. 2018), using a 1" search radius. The result was a sample of 757 stars with rotation periods, parallaxes and *Gaia G*, G_{BP} and G_{RP}-band photometry. Figure 6 shows the rotation periods of Praesepe members as a function of their *Gaia* $G_{BP} - G_{RP}$ colors. The GK and early M dwarfs ($G_{BP} - G_{RP} < 2.4$) which fall on a 'rotational main sequence' are shown as blue points and the late M dwarfs ($G_{BP} - G_{RP} > 2.4$) whose rotation periods are not well determined by their age and color are shown as orange open circles. We excluded the late M dwarfs (orange circles with $G_{BP} - G_{RP} > 2.4$) from this analysis since they do not follow a simple gyrochronology relation however, we included more massive outliers (orange circles with $G_{BP} - G_{RP} < 2.4$) in order to provide a complete picture of the precision and accuracy of gyrochronology applied to Praesepe. Figure 6 shows two sets of gyrochronology models: one calibrated using several open clusters, asteroseismic stars and the Sun (Angus et al. 2015), which was used to infer the ages of Praesepe but clearly does not provide a perfect fit to this cluster (solid gray line), and one fit to Praesepe and the Sun only, as described in section 2, that was used to calculate the Fisher information (dashed black line). We did not account for extinction in our analysis since Praesepe is relatively nearby (around 180 parsecs) so reddening from dust is minimal.

The resulting probability density functions over age predicted for individual members of Praesepe, where each member was treated as an isolated field star, are shown in figure **??**. The orange distributions show posterior PDFs over age for each member of Praesepe, where ages were inferred using isochrone fitting *only*, with *Gaia* colors ($G_{BP} - G_{RP}$), *Gaia* apparent magnitude (G), and *Gaia* parallaxes as the observable properties. The blue distributions are posterior PDFs over stellar age for each member of Praesepe, where ages were inferred using isochrone fitting *and* a gyrochronology model (equation 13). The blue posteriors are much more strongly peaked around the literature age of the cluster (650 Myrs, indicated by a vertical black line) and this demonstrates that rotation periods carry far more age information than photometric colors, even when precise parallaxes are available.

In summary, fitting our new age model to simulated stars and members of the Praesepe cluster (an open cluster with a precisely measured age from ensemble isochrone fitting and MS turn-off) demonstrates that using isochrone fitting *alone* to calculate the ages of cool MS field stars results in extremely imprecise ages, however when gyrochonology is incorporated, the precision of age measurements increase significantly.

Fig. 4.— The results of a test in which we simulated observable properties of stars with the same model we used to infer their properties. In this experiment we used *only* isochrone fitting to infer ages; we did not use rotation periods/gyrochronology. For results where we used *both* stellar evolution models *and* gyrochronology, see figure 5. The true age, used to produce associated observables is shown on the x-axis, and the inferred ages are shown on the y-axis. This figure shows the posterior PDFs over stellar age for each of the simulated stars as a 'violin plot', where samples from the posterior are plotted vertically as a smooth, symmetric function. The widths of these functions indicates the probability density over age: wider regions indicated greater probability mass. The median values of the posterior PDFs are plotted as solid horizontal lines. This figure demonstrates that when only stellar evolution models are used to infer ages for field MS stars, the resulting predicted ages are extremely imprecise.
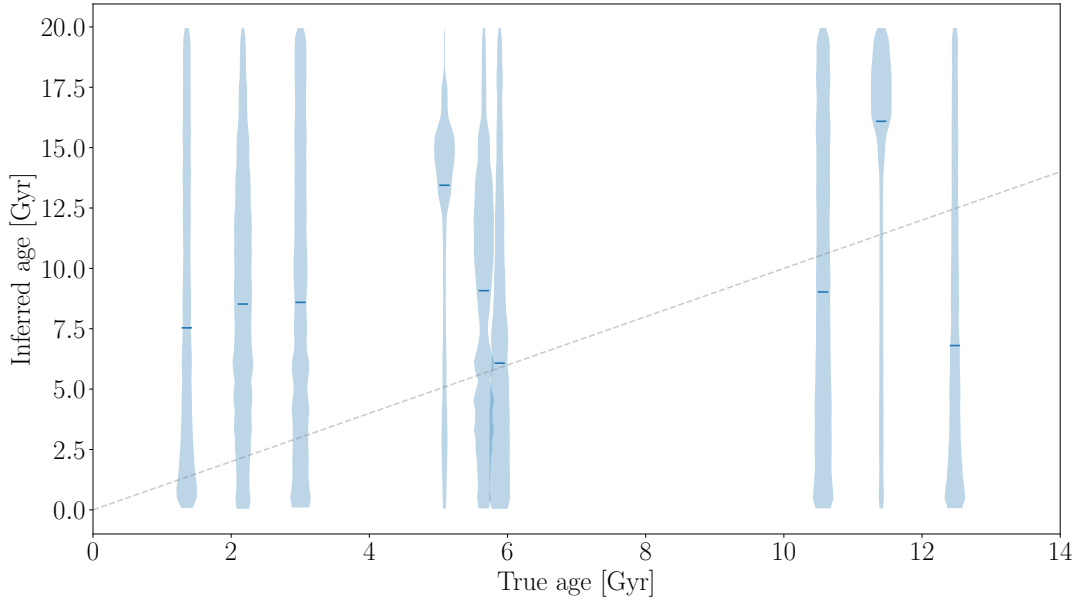
Fig. 5.— The results of a test in which we simulated observable properties of stars with the same model we used to infer their properties. In this experiment we used both isochrone fitting *and* gyrochronology to infer ages. For results where we used stellar evolution models *only*, see the previous figure (figure 4). The true age, used to produce associated observables is shown on the x-axis, and the inferred ages are shown on the y-axis. This figure shows the posterior PDFs over stellar age for each of the simulated stars as a 'violin plot', where samples from the posterior are plotted vertically as a smooth, symmetric function. The widths of these functions indicates the age probability density: wider regions represent greater probability mass. The median values of the posterior PDFs are plotted as solid horizontal lines. This figure demonstrates that when rotation periods (gyrochronology) *and* stellar evolution models are used to infer the ages of field MS stars, the resulting predicted ages are much more precise than isochrone fitting can provide alone. I am rerunning code to fix the outliers in this figure – I think it's an initialization issue. I am also planning to combine this figure with the figure above.
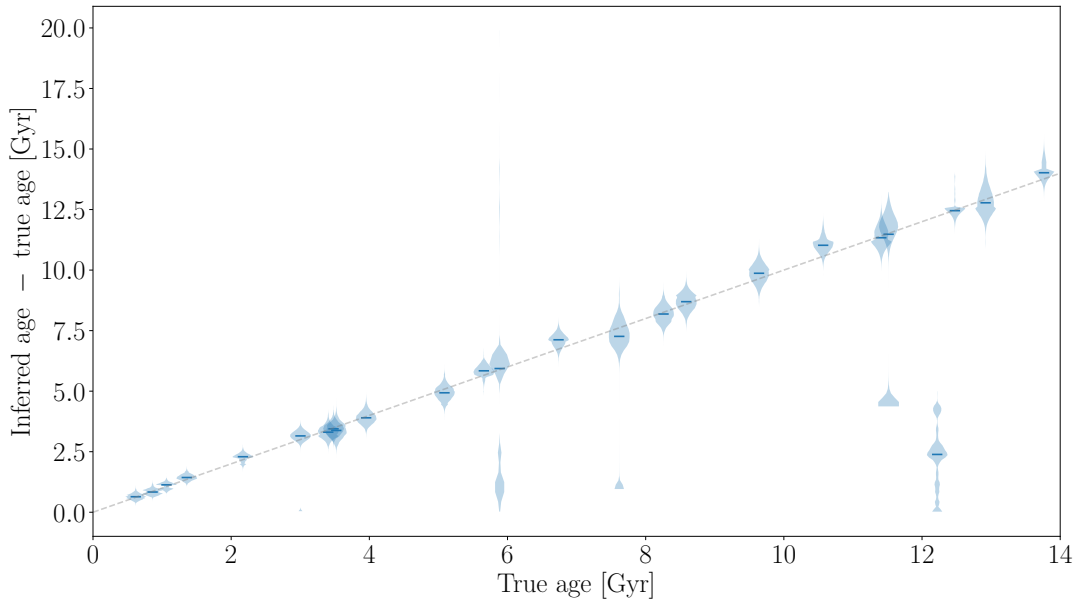
Fig. 6.— The rotation periods of Praesepe members (Douglas et al. 2016), plotted against their *Gaia* colors ($G_{BP} - G_{RP}$) in logarithmic space. GK and early M dwarfs ($G_{BP} - G_{RP}$ < 2.4), shown as blue points fall on a 'rotational main sequence' whereas the rotation periods of late M dwarfs ($2.4 < G_{BP} - G_{RP}$), shown as orange open circles are noisy and not strongly predicted by their age and color. We excluded late M dwarfs from our age analysis of Praesepe stars. We excluded outliers at earlier spectral types, also shown as open orange circles at colors less than 2.4, to perform the polynomial fit to Praesepe described in section 2 (resulting in the black dashed line) but included these outliers when inferring the ages of Praesepe stars in section 4. The early-type outliers were identified via sigma-clipping at 4.5σ. The black-dashed model was used to calculate the Fisher information shown in figures 1 and 2. The solid gray lines show gyrochrones that were calibrated using the Hyades, Coma Berenices and Pleiades clusters, as well as the Sun and *Kepler* asteroseismic stars (Angus et al. 2015), and used to predict the ages of Praesepe stars, shown in figure 7. This model does not provide a perfect fit to Praesepe (Praesepe was not used to calibrate it), particularly for the hottest and coolest stars, however this is the current gyrochronology model implemented in our joint isochrone fitting and gyrochronology model. This figure was generated in a *Jupyter* notebook available at this url: https://github.com/RuthAngus/stardate/blob/master/paper/code/Praesepe.ipynb
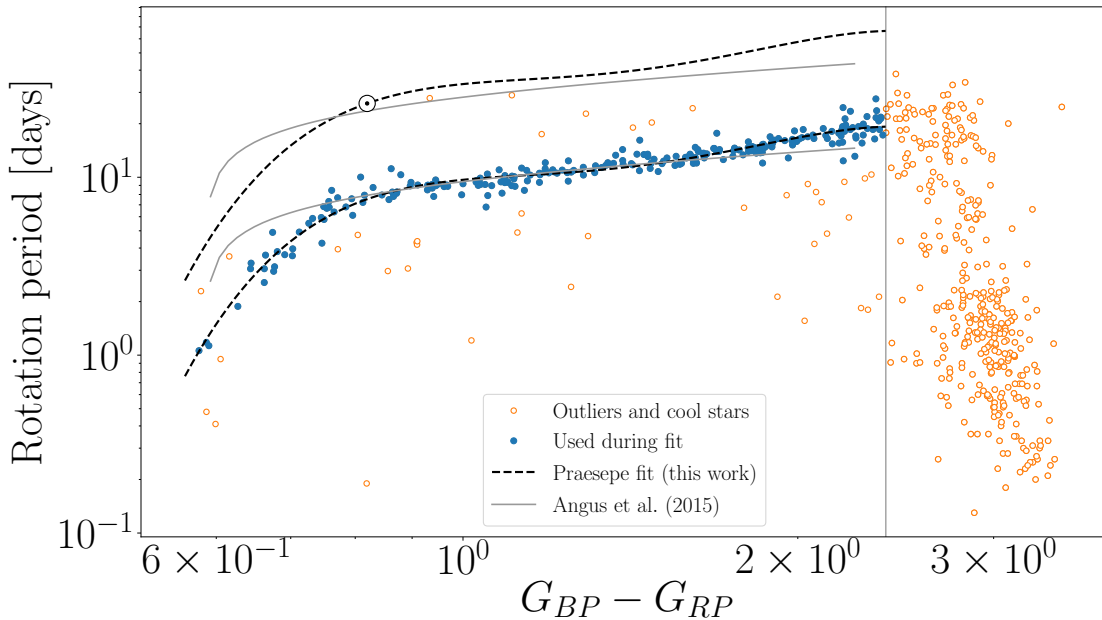
Fig. 7.— The unnormalized posterior PDFs over the ages of Praesepe stars inferred using an isochrone fitting method (orange) and a joint isochrone fitting and gyrochronology model (blue). MIST isochrones were used for isochrone fitting and the gyrochronology model is shown as solid grey lines in figure 6 (Angus et al. 2015). The black line shows the established age of Praesepe (650 Myrs). The blue posterior PDFs are more strongly peaked around the established age for Praesepe than the orange, indicating that gyrochronology is much more informative for these MS stars than isochrone fitting. Still need to quantify the improvement
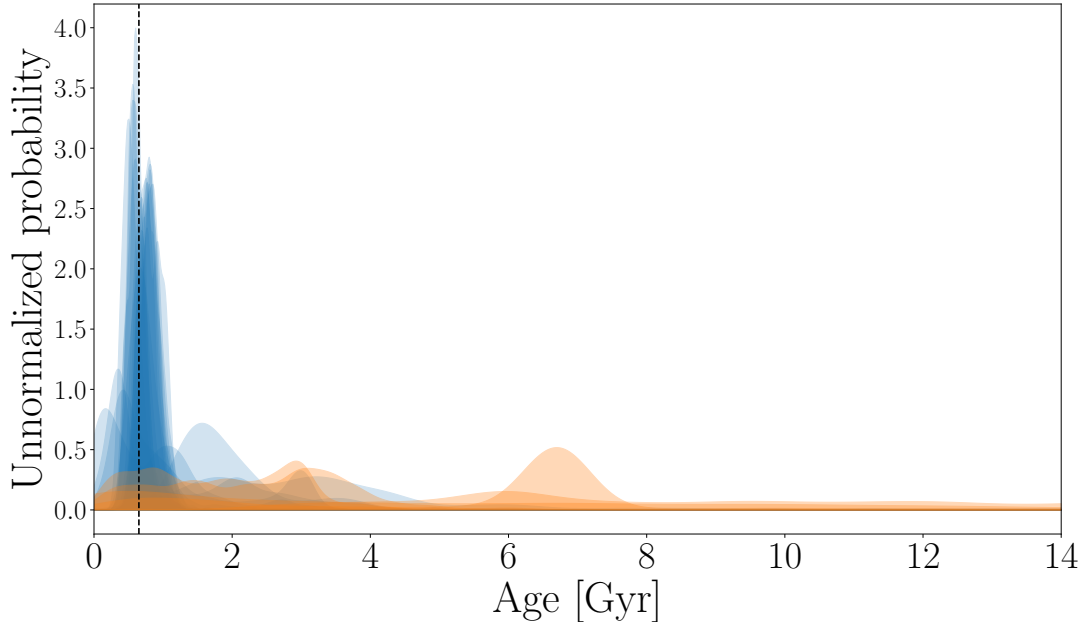
5. Discussion

In the previous sections we demonstrated that modeling the ages of stars using isochrones *and* gyrochronology can result in more precise and accurate ages than using isochrone fitting alone. Isochrone fitting and gyrochronology are complementary because gyrochronology is more precise where isochrone fitting is less precise (on the MS) and vice versa (at MS turn off). Age precision is determined by the spacing of isochrones or gyrochrones: in regions where iso/gyrochrones are more tightly spaced, ages will be less precise. Isochrones become less tightly spaced (and more precise) at larger stellar masses and lower surface gravities. Gyrochrones become more tightly spaced (and less precise) at larger stellar masses.

The method we present here is available as a *python* package called `stardate` which allows users to infer ages from their apparent magnitudes, parallaxes, rotation periods and spectroscopic propertes, if available, in just a few lines of code. This method is applicable to an extremely large number of stars: most stars with a rotation period and broad-band photometry, which already includes tens-of-thousands *Kepler* and *K2* stars and could include millions from *TESS, LSST, WFIRST, PLATO, Gaia*, and others. Although this method is designed for combining isochrone fitting with gyrochronology, `stardate` can still be used *without* rotation periods, in which case it will predict an isochrone-only stellar age. `stardate` is therefore applicable to all stars covered by the MIST isochrones: masses from 0.1 to 300 $M_\odot$, ages ranging from 100,000 years to longer than the age of the Universe, and metallicities from -4 to 0.5, however it is *optimally applicable* to stars with rotation periods, otherwise the result will be identical to ages measured with `isochrones.py`. However, there are some types of star for which our combined isochrone fitting and gyrochronology model should either be used with caution or should not be applied. This list includes: fully convective stars with $G_{BP} - G_{RP} > 2.4$, or less massive than around 0.3 $M_\odot$, stars younger than around 500 Myrs where there is a significant number of rapidly rotating outliers, stars that have stopped magnetic braking, *i.e.* those with *Ro* greater than around 2.1; and synchronised binaries whose rotation periods are locked to their orbital periods. In addition, any given star, even if it does meet the criteria for mass, age, binarity, etc, may still be a rotational outlier. Rotational outliers are often seen in clusters (see *e.g.* Douglas et al. 2016; Rebull et al. 2016; Douglas et al. 2017; Rebull et al. 2017). When a star's age is not accurately represented by its rotation period, its isochronal age will be in tension with its gyrochronal one, however, given the precision of the gyrochronal technique, the gyrochronal age will dominate. In addition, measured rotation periods may not always be accurate and in many cases, due to aliasing, can be a harmonic of the true rotation period. A common rotation period measurement failure mode is to measure half the true rotation period. The best way to prevent an erroneous or outlying rotation period from resulting in an erroneous age measurement is to *allow* for outlying rotation periods using a mixture model. Finally, as

shown in figure 6 the gyrochronology model used here (Angus et al. 2015) does not provide a good fit to all available data. In future we intend to recalibrate this model so that it fits all available cluster and asteroseismic data. We also intend to build methods to account for and accommodate outliers, old stars and low-mass stars. For now however, we simply warn users of these caveats and suggest that ages calculated using `stardate` are treated with appropriate caution.

6.   Conclusion

We present a statistical framework for measuring precise ages of MS stars and subgiants by combining observables that relate, via different evolutionary processes, to stellar age. Specifically, we combine information used to place stars on an isochrone in an HR diagram or CMD (T_{eff}, log(g), observed bulk metallicity, parallax and photometric colors) with rotation periods which are used to date stars via their magnetic braking history (gyrochronology). The two methods of isochrone fitting and gyrochronology are combined by taking the product of two likelihoods: one that contains an isochronal model and the other a gyrochronal one. We used the MIST stellar evolution models and computed isochronal ages and likelihoods using the `isochrones.py` *Python* package. The gyrochronal model is a power-law relation between rotation period, B-V color and age, based on the functional form first introduced by Barnes (2003) and later recalibrated by Angus et al. (2015). We tested this age-dating model, called `stardate` on simulated data and cluster stars with precisely measured ages. We found that combining isochrone fitting and gyrochronology predicts ages that are an order of magnitude more precise than using isochrone fitting alone, confirming predictions made using information theory. Gyrochronology and isochrone fitting are also extremely complementary: gyrochronology supplies precise ages on the main sequence and isochrone fitting provides precise ages near main sequence turn off. `stardate` allows users to infer precise ages for MS stars and subgiants alike, without having to first identify the age-dating method that is best for any given star: `stardate` automatically infers the most precise possible age. However, we caution users that the gyrochronology model currently built into `stardate` does not provide a good fit to all data and is not suitable for low mass stars or those who may have ceased magnetic braking. In the future we hope to make several improvements to the gyrochronology relation implemented in `stardate` that will make it applicable to *all* MS and subgiant stars.

The code used in this project is available as a documented *python* package called `stardate`. It is available for download via Github[6] or through PyPI[7]. Documentation is available at https://stardate.readthedocs.io/en/latest/. All code used to produce the figures in this paper is available at https://github.com/RuthAngus/stardate. add github hash.

---

[6] git clone https://github.com/RuthAngus/stardate.git

[7] pip install stardate_code

7. Appendix

Priors

We use the default priors in the `isochrones.py` *python* package. The prior over age is,

$$p(A) = \frac{\log(10)10^A}{10^{10.5} - 10^8}, \quad 8 < A < 10.5. \tag{19}$$

where A, is $\log_{10}(\text{Age [yrs]})$. The prior over mass is uniform in natural-log between -20 and 20,

$$p(M) = U(-20, 20) \tag{20}$$

where M is $\ln(\text{Mass } [M_\odot])$. The prior over true bulk metallicity is based on the galactic metallicity distribution, as inferred using data from the Sloan Digital Sky Survey citation. It is the product of a Gaussian that describes the metallicity distribution over halo stars and two Gaussians that describe the metallicity distribution in the thin and thick disks:

$$p(F) = H_F \frac{1}{\sqrt{2\pi\sigma_{\text{halo}}^2}} \exp\left(-\frac{(F-\mu_{\text{halo}})^2}{2\sigma_{\text{halo}}}\right) \tag{21}$$
$$\times (1 - H_F)\frac{1}{\xi}\left[\frac{0.8}{0.15} \exp\left(-\frac{(F-0.016)^2}{2\times0.15^2}\right) + \frac{0.2}{0.22}\exp\left(-\frac{(F-0.15)^2}{2\times0.22^2}\right)\right],$$

where $H_F = 0.001$ is the halo fraction, μ_{halo} and σ_{halo} are the mean and standard deviation of a Gaussian that describes a probability distribution over metallicity in the halo, and take values -1.5 and 0.4 respectively. The two Gaussians inside the square brackets describe probability distributions over metallicity in the thin and thick disks. The values of the means and standard deviations in these Gaussians are from **?**. ξ is the integral of everything in the square brackets from $-\infty$ to ∞ and takes the value ~ 2.507. The prior over distance is,

$$p(D) = \frac{3}{3000^3}D^2, \quad 0 < D < 3000, \tag{22}$$

where D is in kiloparsecs. Finally, the prior over extinction is uniform between zero and one,

$$p(A_V) = U(0, 1). \tag{23}$$

REFERENCES

R. Angus, S. Aigrain, D. Foreman-Mackey, and A. McQuillan. Calibrating gyrochronology using Kepler asteroseismic targets. *MNRAS*, 450:1787–1798, June 2015. doi: 10.1093/mnras/stv423.

H. Balthasar, M. Vazquez, and H. Woehl. Differential rotation of sunspot groups in the period from 1874 through 1976 and changes of the rotation velocity within the solar cycle. *A&A*, 155:87–98, January 1986.

S. A. Barnes. On the Rotational Evolution of Solar- and Late-Type Stars, Its Magnetic Origins, and the Possibility of Stellar Gyrochronology. *ApJ*, 586:464–479, March 2003. doi: 10.1086/367639.

S. A. Barnes. Ages for Illustrative Field Stars Using Gyrochronology: Viability, Limitations, and Errors. *ApJ*, 669:1167–1189, November 2007. doi: 10.1086/519295.

C. J. Burke, J. L. Christiansen, F. Mullally, S. Seader, D. Huber, J. F. Rowe, J. L. Coughlin, S. E. Thompson, J. Catanzarite, B. D. Clarke, T. D. Morton, D. A. Caldwell, S. T. Bryson, M. R. Haas, N. M. Batalha, J. M. Jenkins, P. Tenenbaum, J. D. Twicken, J. Li, E. Quintana, T. Barclay, C. E. Henze, W. J. Borucki, S. B. Howell, and M. Still. Terrestrial Planet Occurrence Rates for the Kepler GK Dwarf Sample. *ApJ*, 809:8, August 2015. doi: 10.1088/0004-637X/809/1/8.

L. Casagrande and D. A. VandenBerg. On the use of Gaia magnitudes and new tables of bolometric corrections. *MNRAS*, 479:L102–L107, September 2018. doi: 10.1093/mnrasl/sly104.

J. Choi, A. Dotter, C. Conroy, M. Cantiello, B. Paxton, and B. D. Johnson. Mesa Isochrones and Stellar Tracks (MIST). I. Solar-scaled Models. *ApJ*, 823:102, June 2016. doi: 10.3847/0004-637X/823/2/102.

J. N. Connelly, M. Bizzarro, A. N. Krot, Å. Nordlund, D. Wielandt, and M. A. Ivanova. The Absolute Chronology and Thermal Processing of Solids in the Solar Protoplanetary Disk. *Science*, 338:651, November 2012. doi: 10.1126/science.1226919.

A. Dotter. MESA Isochrones and Stellar Tracks (MIST) 0: Methods for the Construction of Stellar Isochrones. *ApJS*, 222:8, January 2016. doi: 10.3847/0067-0049/222/1/8.

A. Dotter, B. Chaboyer, D. Jevremović, V. Kostov, E. Baron, and J. W. Ferguson. The Dartmouth Stellar Evolution Database. *ApJS*, 178:89–101, September 2008. doi: 10.1086/589654.

S. T. Douglas, M. A. Agüeros, K. R. Covey, P. A. Cargile, T. Barclay, A. Cody, S. B. Howell, and T. Kopytova. K2 Rotation Periods for Low-mass Hyads and the Implications for Gyrochronology. *ApJ*, 822:47, May 2016. doi: 10.3847/0004-637X/822/1/47.

S. T. Douglas, M. A. Agüeros, K. R. Covey, and A. Kraus. Poking the Beehive from Space: K2 Rotation Periods for Praesepe. *ApJ*, 842:83, June 2017. doi: 10.3847/1538-4357/aa6e52.

D. Foreman-Mackey, D. W. Hogg, D. Lang, and J. Goodman. emcee: The MCMC Hammer. *PASP*, 125:306, March 2013. doi: 10.1086/670067.

D. Foreman-Mackey, D. W. Hogg, and T. D. Morton. Exoplanet Population Inference and the Abundance of Earth Analogs from Noisy, Incomplete Catalogs. *ApJ*, 795:64, November 2014. doi: 10.1088/0004-637X/795/1/64.

L. Fossati, S. Bagnulo, J. Landstreet, G. Wade, O. Kochukhov, R. Monier, W. Weiss, and M. Gebran. The effect of rotation on the abundances of the chemical elements of the A-type stars in the Praesepe cluster. *A&A*, 483:891–902, June 2008. doi: 10.1051/0004-6361:200809467.

Gaia Collaboration, A. G. A. Brown, A. Vallenari, T. Prusti, J. H. J. de Bruijne, C. Babusiaux, C. A. L. Bailer-Jones, M. Biermann, D. W. Evans, L. Eyer, and et al. Gaia Data Release 2. Summary of the contents and survey properties. *A&A*, 616:A1, August 2018. doi: 10.1051/0004-6361/201833051.

S. Gossage, C. Conroy, A. Dotter, J. Choi, P. Rosenfield, P. Cargile, and A. Dolphin. Age Determinations of the Hyades, Praesepe, and Pleiades via MESA Models with Rotation. *ApJ*, 863:67, August 2018. doi: 10.3847/1538-4357/aad0a0.

R. Howe, J. Christensen-Dalsgaard, F. Hill, R. W. Komm, R. M. Larsen, J. Schou, M. J. Thompson, and J. Toomre. Dynamic Variations at the Base of the Solar Convection Zone. *Science*, 287:2456–2460, March 2000. doi: 10.1126/science.287.5462.2456.

J. Irwin and J. Bouvier. The rotational evolution of low-mass stars. In E. E. Mamajek, D. R. Soderblom, and R. F. G. Wyse, editors, *The Ages of Stars*, volume 258 of *IAU Symposium*, pages 363–374, June 2009. doi: 10.1017/S1743921309032025.

S. D. Kawaler. Angular momentum loss in low-mass stars. *ApJ*, 333:236–247, October 1988. doi: 10.1086/166740.

S. D. Kawaler. Rotational dating of middle-aged stars. *ApJ*, 343:L65–L68, August 1989. doi: 10.1086/185512.

E. E. Mamajek and L. A. Hillenbrand. Improved Age Estimation for Solar-Type Dwarfs Using Activity-Rotation Diagnostics. *ApJ*, 687:1264–1293, November 2008. doi: 10.1086/591785.

A. W. Mann, E. Gaidos, A. Vanderburg, A. C. Rizzuto, M. Ansdell, J. V. Medina, G. N. Mace, A. L. Kraus, and K. R. Sokal. Zodiacal Exoplanets in Time (ZEIT). IV. Seven Transiting Planets in the Praesepe Cluster. *AJ*, 153:64, February 2017. doi: 10.1088/1361-6528/aa5276.

A. W. Mann, A. Vanderburg, A. C. Rizzuto, A. L. Kraus, P. Berlind, A. Bieryla, M. L. Calkins, G. A. Esquerdo, D. W. Latham, G. N. Mace, N. R. Morris, S. N. Quinn, K. R. Sokal, and R. P. Stefanik. Zodiacal Exoplanets in Time (ZEIT). VI. A Three-planet System in the Hyades Cluster Including an Earth-sized Planet. *AJ*, 155:4, January 2018. doi: 10.3847/1538-3881/aa9791.

S. P. Matt, A. S. Brun, I. Baraffe, J. Bouvier, and G. Chabrier. The Mass-dependence of Angular Momentum Evolution in Sun-like Stars. *ApJ*, 799:L23, January 2015. doi: 10.1088/2041-8205/799/2/L23.

A. McQuillan, T. Mazeh, and S. Aigrain. Rotation Periods of 34,030 Kepler Main-sequence Stars: The Full Autocorrelation Sample. *ApJS*, 211:24, April 2014. doi: 10.1088/0067-0049/211/2/24.

B. Paxton, L. Bildsten, A. Dotter, F. Herwig, P. Lesaffre, and F. Timmes. Modules for Experiments in Stellar Astrophysics (MESA). *ApJS*, 192:3, January 2011. doi: 10.1088/0067-0049/192/1/3.

B. Paxton, M. Cantiello, P. Arras, L. Bildsten, E. F. Brown, A. Dotter, C. Mankovich, M. H. Montgomery, D. Stello, F. X. Timmes, and R. Townsend. Modules for Experiments in Stellar Astrophysics (MESA): Planets, Oscillations, Rotation, and Massive Stars. *ApJS*, 208:4, September 2013. doi: 10.1088/0067-0049/208/1/4.

B. Paxton, P. Marchant, J. Schwab, E. B. Bauer, L. Bildsten, M. Cantiello, L. Dessart, R. Farmer, H. Hu, N. Langer, R. H. D. Townsend, D. M. Townsley, and F. X. Timmes. Modules for Experiments in Stellar Astrophysics (MESA): Binaries, Pulsations, and Explosions. *ApJS*, 220:15, September 2015. doi: 10.1088/0067-0049/220/1/15.

B. Paxton, J. Schwab, E. B. Bauer, L. Bildsten, S. Blinnikov, P. Duffell, R. Farmer, J. A. Goldberg, P. Marchant, E. Sorokina, A. Thoul, R. H. D. Townsend, and F. X. Timmes. Modules for Experiments in Stellar Astrophysics (MESA): Convective Boundaries, Element Diffusion, and Massive Star Explosions. *ApJS*, 234:34, February 2018. doi: 10.3847/1538-4365/aaa5a8.

M. A. C. Perryman, A. G. A. Brown, Y. Lebreton, A. Gomez, C. Turon, G. Cayrel de Strobel, J. C. Mermilliod, N. Robichon, J. Kovalevsky, and F. Crifo. The Hyades: distance, structure, dynamics, and age. *A&A*, 331:81–120, March 1998.

E. A. Petigura, A. W. Howard, and G. W. Marcy. Prevalence of Earth-size planets orbiting Sun-like stars. *Proceedings of the National Academy of Science*, 110:19273–19278, November 2013. doi: 10.1073/pnas.1319909110.

L. M. Rebull, J. R. Stauffer, J. Bouvier, A. M. Cody, L. A. Hillenbrand, D. R. Soderblom, J. Valenti, D. Barrado, H. Bouy, D. Ciardi, M. Pinsonneault, K. Stassun, G. Micela, S. Aigrain, F. Vrba, G. Somers, J. Christiansen, E. Gillen, and A. Collier Cameron. Rotation in the Pleiades with K2. I. Data and First Results. *AJ*, 152:113, November 2016. doi: 10.3847/0004-6256/152/5/113.

L. M. Rebull, J. R. Stauffer, L. A. Hillenbrand, A. M. Cody, J. Bouvier, D. R. Soderblom, M. Pinsonneault, and L. Hebb. Rotation of Late-type Stars in Praesepe with K2. *ApJ*, 839:92, April 2017. doi: 10.3847/1538-4357/aa6aa4.

A. C. Rizzuto, A. Vanderburg, A. W. Mann, A. L. Kraus, C. D. Dressing, M. A. Agüeros, S. T. Douglas, and D. M. Krolikowski. Zodiacal Exoplanets in Time (ZEIT). VIII. A Two-planet System in Praesepe from K2 Campaign 16. *AJ*, 156:195, November 2018. doi: 10.3847/1538-3881/aadf37.

A. Skumanich. Time Scales for CA II Emission Decay, Rotational Braking, and Lithium Depletion. *ApJ*, 171:565, February 1972. doi: 10.1086/151310.

D. R. Soderblom. The Ages of Stars. *ARA&A*, 48:581–629, September 2010. doi: 10.1146/annurev-astro-081309-130806.

J. L. van Saders and M. H. Pinsonneault. Fast Star, Slow Star; Old Star, Young Star: Subgiant Rotation as a Population and Stellar Physics Diagnostic. *ApJ*, 776:67, October 2013. doi: 10.1088/0004-637X/776/2/67.

J. L. van Saders, T. Ceillier, T. S. Metcalfe, V. Silva Aguirre, M. H. Pinsonneault, R. A. García, S. Mathur, and G. R. Davies. Weakened magnetic braking as the origin of anomalously rapid rotation in old field stars. *Nature*, 529:181–184, January 2016. doi: 10.1038/nature16168.

A. Vanderburg, A. W. Mann, A. Rizzuto, A. Bieryla, A. L. Kraus, P. Berlind, M. L. Calkins, J. L. Curtis, S. T. Douglas, G. A. Esquerdo, M. E. Everett, E. P. Horch, S. B. Howell, D. W. Latham, A. W. Mayo, S. N. Quinn, N. J. Scott, and R. P. Stefanik. Zodiacal Exoplanets in Time (ZEIT). VII. A Temperate Candidate Super-Earth in the Hyades Cluster. *AJ*, 156:46, August 2018. doi: 10.3847/1538-3881/aac894.

D. Veras, D. J. A. Brown, A. J. Mustill, and D. Pollacco. Prospects for detecting decreasing exoplanet frequency with main-sequence age using PLATO. *MNRAS*, 453:67–72, October 2015. doi: 10.1093/mnras/stv1615.

S. Yi, P. Demarque, Y.-C. Kim, Y.-W. Lee, C. H. Ree, T. Lejeune, and S. Barnes. Toward Better Age Estimates for Stellar Populations: The Y^2 Isochrones for Solar Mixture. *ApJS*, 136:417–437, October 2001. doi: 10.1086/321795.